

FMC-DETR: Frequency-Decoupled Multi-Domain Coordination for Aerial-View Object Detection

Ben Liang, Yuan Liu, Bingwen Qiu, Yihong Wang, Xiubao Sui, and Qian Chen

Abstract—Aerial-view object detection is a critical technology for real-world applications such as natural resource monitoring, traffic management, and UAV-based search and rescue. Detecting tiny objects in high-resolution aerial imagery presents a long-standing challenge due to their limited visual cues and the difficulty of modeling global context in complex scenes. Existing methods are often hampered by delayed contextual fusion and inadequate non-linear modeling, failing to effectively use global information to refine shallow features and thus encountering a performance bottleneck. To address these challenges, we propose FMC-DETR, a novel framework with frequency-decoupled fusion for aerial-view object detection. First, we introduce the Wavelet Kolmogorov-Arnold Transformer (WeKat) backbone, which applies cascaded wavelet transforms to enhance global low-frequency context perception in shallow features while preserving fine-grained details, and employs Kolmogorov-Arnold networks to achieve adaptive non-linear modeling of multi-scale dependencies. Next, a lightweight Cross-stage Partial Fusion (CPF) module reduces redundancy and improves multi-scale feature interaction. Finally, we introduce the Multi-Domain Feature Coordination (MDFC) module, which unifies spatial, frequency, and structural priors to balance detail preservation and global enhancement. Extensive experiments on benchmark aerial-view datasets demonstrate that FMC-DETR achieves state-of-the-art performance with fewer parameters. On the challenging VisDrone dataset, our model achieves improvements of 6.5% AP and 8.2% AP₅₀ over the baseline, highlighting its effectiveness in tiny object detection. The code can be accessed at <https://github.com/bloomingvision/FMC-DETR>

Index Terms—Object detection, aerial imagery, frequency-decoupled fusion, multi-scale feature.

I. INTRODUCTION

Object detection, a cornerstone task in computer vision, has demonstrated profound utility in a multitude of industrial applications, including autonomous driving [1], [2], remote sensing [3], [4], and urban surveillance [5], [6]. Propelled by the rapid advances in deep learning, particularly Convolutional Neural Networks (CNNs), modern detection frameworks have achieved remarkable success on natural images at relatively low resolution. However, their performance drops sharply on high-resolution aerial imagery, where objects are typically small, weakly featured, randomly distributed, and frequently occluded [7].

This work was supported by the National Natural Science Foundation of China under Grant 62301253 and Grant 62427818. (Corresponding author: Yuan Liu and Xiubao Sui.)

Ben Liang, Yuan Liu, Bingwen Qiu, Yihong Wang, Xiubao Sui, and Qian Chen are with the School of Electronic Engineering and Optoelectronic Technology, Nanjing University of Science and Technology, Nanjing 210094, China (e-mail: benliang@njust.edu.cn; lyuan90_eo@njust.edu.cn; qbw0315@njust.edu.cn; h@njust.edu.cn; sxb@njust.edu.cn; chenqian@njust.edu.cn).

To mitigate the challenge of limited appearance information, enhancing the model's perception of global context has emerged as a critical research direction [8], [9]. CNNs, while serving as the default backbone architecture due to their potent local feature extraction capabilities, are constrained by an inherent local inductive bias. Their progressively stacked convolutional layers result in a slowly expanding receptive field, fundamentally limiting their capacity to model the long-range dependencies (LRDs) essential for contextual reasoning. This limitation is particularly disadvantageous for small objects, as distinguishing objects in complex backgrounds requires a comprehensive understanding of the overall scene structure. To transcend the locality of CNNs, researchers have increasingly turned to Transformer-based architectures [10]–[12], which leverage self-attention mechanisms to explicitly capture LRDs. However, the computational complexity of Transformers scales quadratically ($O(N^2)$) with respect to the number of input tokens, making their direct application to high-resolution feature maps computationally prohibitive. As a result, a common solution is to adopt a hybrid architecture, where CNNs process high-resolution shallow layers and Transformers are reserved for low-resolution deeper layers. However, this design introduces a critical performance bottleneck. Shallow feature maps—rich in spatial detail and fine-grained structures—are vital for detecting tiny objects, yet they are processed by modules with limited global modeling capacity. Postponing global context modeling to deeper layers often leads to the degradation or loss of discriminative cues for small objects due to successive downsampling.

Furthermore, we identify a more fundamental yet often overlooked limitation in how current Transformer models conceptualize contextual integration: they fail to adequately capture the inherently non-linear nature of contextual dependencies. This inadequacy stems from the reliance on Multi-Layer Perceptrons (MLPs) with static, data-agnostic activation functions (e.g., ReLU) for feature transformation. In object detection, however, contextual relationships are profoundly non-linear: 1) Strong Scene-Object Priors: The probability of an object's presence can change abruptly with context—for instance, the likelihood of a ship drops to near zero when transitioning from water to land. Such step-like dependencies cannot be modeled by smooth, linear combinations. 2) Adaptive Cross-Scale Feature Fusion: Fusing semantic information from deep layers with fine-grained details from shallow layers is not a simple weighted average but a dynamic, non-linear process modulated by factors such as object scale and occlusion.

To address these limitations, we propose the FMC-DETR,

a novel framework that enhances tiny object detection by introducing global context modeling into the high-resolution stages and incorporating adaptive non-linear reasoning into the contextual fusion process. First, the WeKat backbone enhances global context awareness while preserving high-frequency details via frequency decoupling. Next, the CPF module efficiently fuses multi-scale features and reduces redundancy. Finally, the MDFC module refines high-resolution multi-scale features via spatial-frequency domain calibration, significantly enhancing the recognition of tiny objects. Extensive experiments on public aerial-view datasets, including VisDrone [13], HazyDet [14], and SIMD [15], demonstrate that FMC-DETR exhibits exceptional competitiveness on tiny object detection tasks. In summary, our main contributions are as follows:

- We introduce WeKat, a hybrid backbone incorporating a novel Heterogeneous Split-Gating (HSG) mechanism to decouple feature flow. HSG-WAVE enables efficient spatial-frequency modeling with near-linear global receptive fields in shallow layers, while HSG-AKAT enhances non-linear semantic abstraction in deeper stages via a content-aware spatial bias and group Kolmogorov-Arnold networks.
- We propose CPF, a lightweight module designed for efficient multi-scale feature aggregation. It selectively applies a powerful reparameterized convolution to part of the channels for spatial feature extraction, effectively reducing inter-channel redundancy.
- We propose the MDFC module to enhance fine-grained feature representation for small object detection. By jointly modeling structural information in the spatial domain and high-frequency cues in the frequency domain, MDFC preserves object integrity while producing more discriminative and robust features for accurate detection.

II. RELATED WORK

A. CNN-Transformer Object Detectors

CNN and Transformer, as the two cornerstones of the visual domain, have given rise to numerous outstanding detection models. YOLO [16]–[21], a mainstream detection framework primarily built on CNNs, achieves a commendable balance between detection accuracy and inference speed. In parallel, frameworks based on Vision Transformers (ViTs) [11] leverage self-attention mechanisms to continuously advance detection accuracy. In recent years, hybrid architectures combining CNNs and Transformers, such as DETR [22], Deformable DETR [23], RT-DETR [24], D-FINE [25], and DEIM [26], have garnered increasing attention. These models utilize convolutional networks for feature extraction and interaction while employing Transformers for object classification and localization, establishing a new and effective collaborative paradigm. Nevertheless, despite their demonstrated success on public benchmarks like COCO with low-resolution natural images, their efficacy falters when applied to high-resolution aerial imagery. This performance degradation is particularly acute for tiny objects, a shortcoming that can be attributed

to their inadequate attention to critical, detail-rich shallow features.

B. Small Object Detection

Detecting small objects has long been challenging. To tackle the persistent challenge of small object detection, recent works have explored various enhancement strategies. GLSAN [8] integrates global-local fusion strategies into a progressive scale-changing network for more accurate bounding box localization. CEASC [5] introduces context-enhanced sparse convolutions to enhance global information, achieving significant improvements in small object detection accuracy. YOLO-DCTI [9] proposes Contextual Transformer (CoT) to integrate global residual and local fusion mechanisms into the detection network, enhancing the contextual utilization of small target pixel information. FBRT-YOLO [7] introduces a Feature Complementary Mapping (FCM) module that integrates semantic and spatial location information, effectively alleviating the loss of small target information and improving small target localization capabilities. Although these methods achieved improvements in enhancing small object detection, none of them took into account the importance of capturing global contextual features at lower levels.

C. Frequency-domain Fusion

Frequency-domain features have attracted considerable attention in object detection due to their ability to reveal intricate structural information across diverse scenes. In contrast to spatial-domain features—typically extracted by conventional convolutions—which model spatial layout and contextual relationships in an implicit and localized manner, frequency-domain analysis offers an explicit and global perspective by decomposing intensity variations into distinct spectral components. SWANet [27] uses wavelet transforms to perform multi-scale decomposition of noise and details in images, effectively improving image quality under low light conditions. ELWNet [28] combines the wavelet transform module with CNNs for feature downsampling, using finite parameters to achieve high-quality multi-level encoded features. SFS-CNet [29] proposes a space-frequency selective convolution, which employs a diversion-perception selection strategy to enhance the diversity and uniqueness of features, thereby improving the performance of SAR target detection. Building upon this trend, we explore the integration of frequency- and spatial-domain features specifically for small object detection.

III. METHOD

In this section, we introduce a novel architectural model named FMC-DETR. As illustrated in Fig 1, FMC-DETR employs a cascaded hierarchical design, consisting of three main stages from a macro perspective: the backbone network extracts feature maps at various scales, the cross-layer feature interaction structure facilitates the fusion of multi-scale contextual information, and the detection head performs both feature classification and bounding box localization.

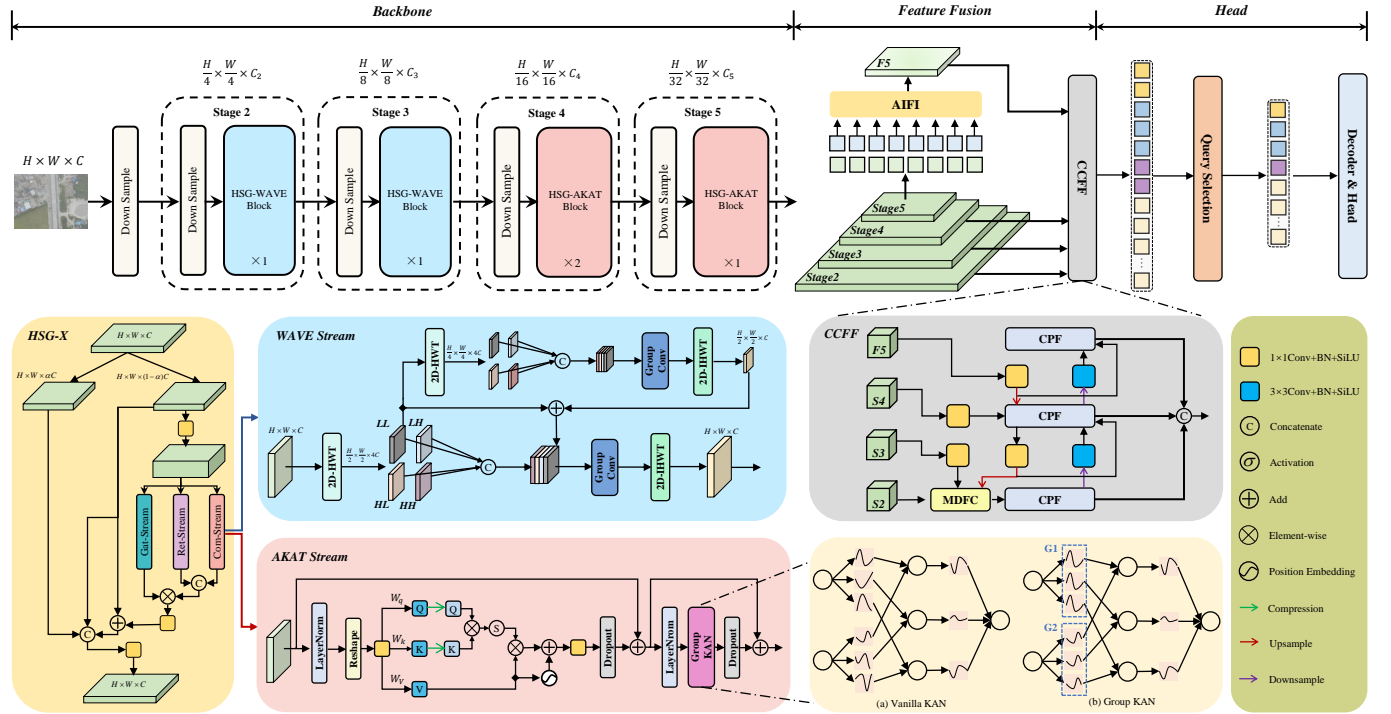


Fig. 1. Overview of the proposed FMC-DETR. The backbone consists of multiple stages to extract and model multi-scale features. Among them, HSG-WAVE and HSG-AKAT are applied to capture correlations in shallow and deep features, respectively. The multi-scale features are then fed into the CCFF structure for feature fusion, within which the CPF module performs efficient feature integration and the MDFC module combines spatial- and frequency-domain information to enhance small-object representation. Finally, the Decoder and Detection Head query the optimized features to produce the final detection results.

A. Wavelet Kolmogorov-Arnold Transformer

In recent years, hybrid architectures that synergistically combine CNNs and Transformers have become a dominant paradigm in backbone network design. Building upon this hybrid philosophy, we propose the Wavelet Kolmogorov-Arnold Transformer (WeKat) backbone, a robust and efficient architecture designed to achieve finer-grained control over internal information flow and mitigate gradient instability in deep networks.

As shown in Fig. 1, WeKat consists of four stages [$S2, S3, S4, S5$], each centered on an innovative Heterogeneous Split-Gating (HSG) structure. The HSG module decomposes the input feature stream into three heterogeneous sub-streams: a Gating Stream (Gat-Stream) for dynamic information modulation, a Retention Stream (Ret-Stream) for lossless information propagation, and a Computation Stream (Com-Stream) for deep feature transformation.

Given an input feature map $X \in \mathbb{R}^{C \times H \times W}$, the HSG restructures the data flow through two successive partitions. (1) Initial Partitioning. The input is divided into X_r and X_p along the channel dimension with a predefined ratio α ($0 < \alpha < 1$). Here, X_r contains the first $C_r = \alpha C$ channels, preserved as an identity mapping path, while X_p contains the remaining $(1 - \alpha)C$ channels, dedicated to complex feature transformations. (2) Re-partitioning. The processing stream X_p undergoes channel expansion and feature remapping via a lightweight 1×1 convolution, after which it is split into three sub-streams:

$$(X_p^g, X_p^r, X_p^c) = \text{Split}(\text{Conv}(X_p)), \quad (1)$$

where X_p^g forms the Gating Stream, generating dynamic content-aware modulation signals; X_p^r represents the Retention Stream, which directly preserves critical features; and X_p^c denotes the Computation Stream (\mathcal{F}) to extract complex patterns and capture spatial relationships. To adapt to different feature hierarchies, we introduce two variants: HSG-WAVE and HSG-KAT.

1) *HSG-WAVE*: CNNs exhibit strong inductive biases such as locality and translation equivariance, which are effective in capturing textures and high-frequency details. However, their limited receptive fields constrain their ability to model global low-frequency structures [30]. To simultaneously preserve fine-grained details and capture holistic shape information in shallow layers, we propose the HSG-WAVE module, which coordinates global structure modeling, spatial-frequency analysis, and multi-frequency feature integration.

Specifically, HSG-WAVE utilizes the Haar Wavelet Transform (HWT) to perform joint spatial-frequency analysis. Given an input feature map X_p^c , the HWT decomposes it into four frequency sub-bands:

$$\text{HWT}(X_p^c) = \{X_p^{cLL^{(l)}}, X_p^{cLH^{(l)}}, X_p^{cHL^{(l)}}, X_p^{cHH^{(l)}}\}, \quad (2)$$

where X_p^{cLL} encodes the low-frequency structural component, while $\{X_p^{cLH}, X_p^{cHL}, X_p^{cHH}\}$ capture high-frequency horizontal, vertical, and diagonal details, respectively. Then, we selectively apply HWT again only to the low-frequency branch (LL) to further encode coarse structural and shape information,

obtaining progressively coarser proxy representations:

$$\text{HWT}(X_p^{cLL^{(l)}}) = \{X_p^{cLL^{(l+1)}}, X_p^{cLH^{(l+1)}}, X_p^{cHL^{(l+1)}}, X_p^{cHH^{(l+1)}}\}, \quad (3)$$

where l denotes the decomposition level. This approach enables the capture of global layout and long-range dependencies while preserving high-frequency sub-bands intact to retain fine textures and edge features. Moreover, operating on successively downsampled LL representations significantly reduces spatial resolution, thereby decreasing computational and memory costs. This allows us to perform more expressive processing on global context with minimal overhead. Then, at each level, all sub-bands are concatenated and processed by a grouped convolution:

$$\hat{X}_p^{c(l+1)} = \text{Conv}_{5 \times 5}^{\text{group}} \left([X_p^{cLL^{(l+1)}}, X_p^{cLH^{(l+1)}}, X_p^{cHL^{(l+1)}}, X_p^{cHH^{(l+1)}}] \right) \quad (4)$$

Subsequently, the Inverse Haar Wavelet Transform (IHWT) reconstructs the spatial representation:

$$R^{(l+1)} = \text{IHWT}(\hat{X}_p^{c(l+1)}). \quad (5)$$

The reconstructed feature map $R^{(l+1)}$ from the deeper layer provides global semantic context, which serves as a rich prior. This prior is then added to the low-frequency component $X_p^{cLL^{(l)}}$ of the current layer.

$$X_p^{c(l)} \leftarrow \text{IHWT}(\hat{X}_p^{cLL^{(l)}} + R^{(l+1)}). \quad (6)$$

The fusion of these two components—global context and local context—enhances the local features with broader, more abstract information, correcting ambiguities caused by limited receptive fields in shallower layers. This coarse-to-fine refinement helps the network better understand object structures at different scales.

Through iterative analysis and synthesis, HSG-WAVE effectively integrates global semantics from the recursively downsampled low-frequency stream with fine local textures from high-frequency components, successfully addressing the dual challenge of global context modeling and detail preservation in shallow layers.

2) *HSG-AKAT*: In the deeper stages of the network, where features transition from structural patterns to semantic abstraction, the Transformer’s global modeling capacity becomes increasingly valuable. However, standard Transformer blocks suffer from two critical limitations: i) the self-attention mechanism incurs high computational cost and flattens spatial features into 1D sequences, thereby disrupting the intrinsic 2D spatial structure; and ii) the MLP layers act as static, data-agnostic mappings, making them prone to overfitting and ineffective at modeling nonlinear contextual dependencies [31]. To overcome these issues, we propose the Asymmetric Kolmogorov-Arnold Transformer (AKAT), a high-performance module tailored to capture global semantics and nonlinear dependencies in deep layers.

a) *Asymmetric Self-Attention*: Given an input feature map $X \in \mathbb{R}^{B \times C \times H \times W}$, we first apply lightweight 1×1 convolutions to generate query, key, and value projections:

$$Q = W_q X, \quad K = W_k X, \quad V = W_v X, \quad (7)$$

where W_q, W_k, W_v are learnable projection matrices. To reduce computational complexity, we employ an asymmetric projection strategy, where the dimensions of the query Q and key K are significantly smaller than that of the value V . This approach minimizes the cost of calculating attention by reducing the number of parameters involved in the key-query interactions, while still preserving the expressiveness of the value representation. To preserve spatial relevance, we introduce a dynamic positional bias derived directly from the value tensor. Specifically, the positional bias P is computed using a depthwise convolution applied to the value tensor V , as shown in the following equation:

$$P = \text{DWConv}_{3 \times 3}(V), \quad (8)$$

where DWConv denotes depthwise convolution. The attention weights are then calculated by adding the positional bias to the scaled dot-product of the query and key:

$$\text{Attn}(Q, K, V) = \text{Softmax} \left(\frac{QK^\top}{\sqrt{d}} + P \right) V, \quad (9)$$

which enables semantic-dependent modulation of neighborhood importance.

b) *Group KAN*: Instead of conventional MLPs, we employ the Kolmogorov-Arnold Network (KAN) [31], which replaces linear transformations with spline-based functional expansions:

$$f(x) = \sum_{m=1}^M \alpha_m \phi_m(x), \quad (10)$$

where $\{\phi_m(\cdot)\}$ are learnable spline basis functions and α_m are trainable coefficients. To improve scalability, we adopt the Group KAN variant [32], where channels are partitioned into G groups, and spline parameters are shared within each group:

$$f_g(x) = \sum_{m=1}^M \alpha_{g,m} \phi_{g,m}(x), \quad g = 1, \dots, G. \quad (11)$$

This reduces parameter overhead while retaining expressive power. Compared to MLPs, Group KAN captures sharp nonlinear dependencies more effectively, while the smoothness of spline bases serves as an implicit regularizer against overfitting.

Overall, HSG-AKAT integrates asymmetric self-attention for efficient global modeling and Group KAN for powerful nonlinear feature transformation, thereby addressing the dual challenges of high computational cost and insufficient nonlinear expressiveness in deep Transformer layers.

B. Cross-stage Partial Fusion

Achieving efficient feature fusion with minimal parameters and computational cost is a central goal in the design of feature interaction structures. As the fundamental component for feature extraction, the standard convolution (Conv) block

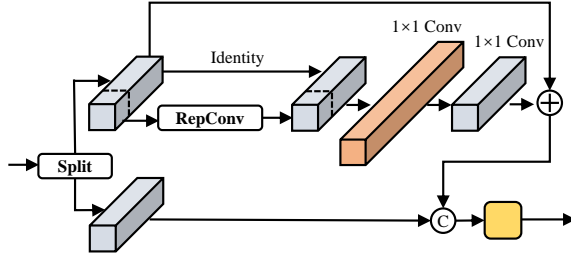


Fig. 2. The overall architecture of CPF.

has inspired numerous variants aimed at improving efficiency. Among the most representative are group convolution (GConv) [33] and depthwise convolution (DWConv) [34], both of which exploit filter redundancy to reduce parameters and FLOPs. In particular, DWConv has been widely adopted due to its substantial savings in parameters and computation. However, a critical challenge is that naively replacing standard convolutions with DWConv often results in a significant drop in accuracy [35]. This limitation has motivated researchers to design novel modules from the perspective of feature map redundancy. Prior studies have demonstrated a high degree of similarity among channels within a feature map, suggesting that applying spatial convolutions to all channels may not be necessary [35]–[37].

To address this issue and improve feature interaction efficiency, we propose the Cross-stage Partial Fusion (CPF) module, a lightweight architecture that maximizes representational power while minimizing computational cost. As shown in Fig 2, instead of performing dense convolutions on all channels, CPF introduces a Partial RepConv (PRConv) for spatial mixing. In PRConv, 3×3 re-parameterized convolutions are selectively applied to 25% of the input channels, while the remaining 75% are preserved through identity mapping. The spatially mixed features are then processed by a channel expansion-and-contraction module, implemented with two successive 1×1 convolutions, which refine the representations in a higher-dimensional space. Finally, the refined features are fused back with the input through a residual connection. By effectively leveraging channel redundancy, CPF achieves a favorable balance between computational efficiency and representational capacity.

C. Multi-Domain Feature Coordination

A central challenge in object detection is the effective fusion of multi-scale features while preserving fine-grained, high-frequency details that are crucial for small object detection. To address this, we propose the Multi-Domain Feature Coordination (MDFC) module, which explicitly unifies spatial, frequency, and structural priors to produce more discriminative feature representations.

MDFC operates in two successive phases: frequency-adaptive modulation and multi-domain refinement. In the first phase, a frequency-adaptive modulation mechanism splits the input feature into spatial and frequency branches. The spatial branch undergoes downsampling to preserve structural integrity, while the frequency branch is transformed

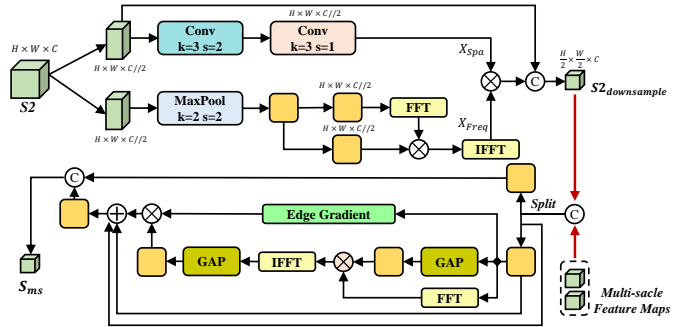


Fig. 3. The overall architecture of MDFC.

into the spectral domain via Fast Fourier Transform (FFT), where element-wise modulation emphasizes informative high-frequency cues. The two branches are then recombined to yield a spatial-frequency enhanced representation. Formally, given an input feature map X_{s2} , MDFC first divides its channels into two parallel paths: a spatial branch X_{s2}^{sp} and a frequency path X_{s2}^{fp} . In the spatial branch, the feature undergoes two convolutions with kernel size 3×3 , where the first convolution has stride $s = 2$ to downsample the feature, and the second convolution has stride $s = 1$ to preserve the spatial layout:

$$\hat{X}_{s2}^{sp} = \text{Conv}_{3 \times 3}^{s=1}(\text{Conv}_{3 \times 3}^{s=2}(X_{s2}^{sp})). \quad (12)$$

In the frequency branch, we first reduce the spatial size using max pooling followed by a 1×1 convolution:

$$X_{mod}^{fp} = \phi(MP(X_{s2}^{fp})), \quad (13)$$

where ϕ denotes the 1×1 convolution. Then, we apply FFT to transform the feature into the frequency domain:

$$\hat{X}_{s2}^{fp} = \mathcal{F}^{-1}\left(\mathcal{F}\left[\phi\left(X_{mod}^{fp(1)}\right)\right] \odot \phi\left(X_{mod}^{fp(2)}\right)\right), \quad (14)$$

where \mathcal{F} and \mathcal{F}^{-1} denotes the FFT and IFFT, respectively. Next, we compute the spatial feature spectrum \hat{X}_{sp} and apply element-wise gating in the frequency domain:

$$\hat{X}_{s2} = \text{Concat}[\hat{X}_{s2}^{sp} \odot \hat{X}_{s2}^{fp}, X_{s2}^{sp}]. \quad (15)$$

In the second phase, the modulated feature is integrated with adjacent multi-scale features and refined across three complementary domains. Specifically, FFT-based global analysis introduces frequency-aware context, GAP-driven channel attention highlights the most informative channels, and Sobel-based gradients provide explicit structural priors to enhance edges and boundaries. By coordinating these orthogonal cues, MDFC encourages global semantics to guide local detail enhancement rather than treating them as independent signals.

Overall, MDFC serves as a cross-domain coordination block that unifies spatial structures, spectral information, and explicit priors. This design endows the detector with strong frequency-awareness and structural sensitivity, substantially improving its ability to recognize small objects without sacrificing efficiency.

IV. EXPERIMENTS

In this section, we first introduce the datasets (VisDrone [13], HazyDet [14], and SIMD [15]) used for aerial-view

object detection. We then describe the experimental settings, followed by comparisons with state-of-the-art methods. Afterwards, ablation studies are conducted to analyze the effectiveness of each component, and the results are further illustrated with qualitative visualizations.

A. Datasets

1) *VisDrone*: VisDrone is a large-scale benchmark specifically designed for object detection in aerial imagery. It consists of high-resolution UAV-captured images from diverse urban and suburban scenes across 14 cities in China, covering a wide range of real-world scenarios. The dataset contains 6,471 training, 548 validation, and 3,190 test images, with over 2.5 million bounding boxes annotated across ten common object categories. Due to the prevalence of small objects, severe occlusions, crowded scenes, and complex backgrounds, VisDrone presents significant challenges for detection algorithms, making it a valuable benchmark for evaluating the robustness and generalization of aerial object detection models.

2) *HazyDet*: HazyDet is the first large-scale benchmark dedicated to object detection in hazy aerial imagery. It contains 11,000 high-resolution images collected from both real-world scenes and physics-based simulations, with 383,000 bounding boxes annotated across three vehicle categories: car, truck, and bus. The dataset is split into 8,000 training, 1,000 validation, and 2,000 test images. By incorporating naturally captured hazy images and synthetic data with varying visibility levels, HazyDet fills a critical gap left by clear-weather benchmarks and provides a valuable resource for evaluating the robustness of detection models under adverse weather conditions.

3) *SIMD*: SIMD is a medium-scale dataset specifically designed for multi-scale and multi-class vehicle detection in satellite imagery. It consists of 5,000 RGB images with a resolution of 1024×768 , collected from 79 locations across Europe and the United States via Google Earth, and adopts a 4:1 training-to-testing split. In total, it provides 45,096 annotated objects spanning 15 categories, mainly vehicles such as cars, trucks, buses, and long vehicles, as well as multiple aircraft types and boats. The diversity in object appearances, scales, densities, and backgrounds makes SIMD a valuable benchmark for advancing aerial object detection, surveillance, and automatic scene analysis under realistic conditions.

B. Implementation Details

All experiments are conducted on an NVIDIA GeForce RTX 4090D GPU. To ensure fair and reproducible comparisons, our method is built upon the RT-DETR [24] baseline and is trained from scratch without using any pretrained weights or additional training strategies, except for Mosaic data augmentation. Unless otherwise specified, the input resolution during both training and testing is fixed at 640×640 . The network is trained for 200 epochs using the AdamW optimizer with a momentum of 0.9, a weight decay of 0.0005, a batch size of 4, and an initial learning rate of 0.0001. We evaluate performance primarily using the COCO-style Average Precision (AP), along with additional AP scores at different thresholds and object scales, including AP_{50} , AP_{75} , AP_S , AP_M , and AP_L .

C. Comparison with state-of-the-arts

1) *Results on VisDrone Dataset*: The results in Table I highlight the superior performance of the proposed FMC-DETR, which establishes a new state-of-the-art on the VisDrone2021 dataset. With an AP of 33.2% and an AP_{50} of 52.8%, FMC-DETR-T achieves the highest accuracy among all compared methods while maintaining a compact model size of 12.6M parameters, demonstrating an excellent balance between efficiency and accuracy. Compared with mainstream YOLO detectors, FMC-DETR achieves consistent improvements. For instance, relative to YOLOv8-X, FMC-DETR-T improves AP and AP_{50} by 4.3% and 6.0% points, respectively, while reducing parameters by 81%. Against the most recent YOLOv12-L and YOLOv13-L, FMC-DETR-T achieves notable gains of +8.8 / +12.3 in AP and +10.8 / +12.3 in AP_{50} , respectively. Moreover, compared with the latest strong CNN-based competitor FBRT-YOLO-X, FMC-DETR achieves superior performance in both AP and AP_{50} while requiring fewer parameters and lower computational cost, surpassing it by 3.1% and 4.4%, respectively. When compared with the strong Transformer-based baseline RT-DETR-R18, FMC-DETR also demonstrates remarkable advantages. Specifically, it achieves improvements of 6.5% in AP and 8.2% in AP_{50} . Furthermore, compared with other advanced algorithms proposed in recent studies, such as Mamba-YOLO and DEIM, FMC-DETR still achieves substantial gains in terms of the AP metric, highlighting its superior detection capability.

2) *Results on HazyDet Dataset*: We compare FMC-DETR-B against several representative object detectors on the challenging HazyDet dataset. As shown in Table II, FMC-DETR-B achieves the highest overall AP of 54.3%, surpassing previous strong baselines such as DeCoDet [14] (52.0%), YOLOv12-L (52.6%), and YOLOv13-L (52.7%). These results underscore the superior detection capability of our method in complex aerial-view scenarios. In terms of category-wise performance, FMC-DETR-B achieves a leading 63.0% AP on the Car class, which dominates the dataset and primarily consists of small, densely packed targets—highlighting the model’s effectiveness in capturing fine-grained details under low-visibility conditions.

3) *Results on SIMD Dataset*: We also evaluate FMC-DETR-B on the SIMD dataset and compare its performance with several recent object detection models. As shown in Table III, FMC-DETR-B achieves an AP of 65.8%, outperforming models like RT-DETR-R18 (63.7%), YOLOv8-L (63.1%), and YOLOv9-M (62.2%), while maintaining a relatively low parameter count of 16.1M and FLOPs of 56.2G. Compared with improved models similar to DETR, FMC-DETR-B achieved the highest AP_{50} , leading Deform DETR [23], EMSD-DETR [40], and HPS-DETR [41] by 6.1%, 1.5%, and 2.3%, respectively.

D. Ablation Studies

To validate the effectiveness of our proposed components, we conducted a comprehensive ablation study on the VisDrone dataset, with the results presented in Table IV.

TABLE I
QUANTITATIVE COMPARISON WITH STATE-OF-THE-ART DETECTORS ON THE VISDRONE2021 VALIDATION SET. **FMC-DETR-BASE (FMC-DETR-B)** REFERS TO THE GENERAL MODEL, AND **FMC-DETR-T (FMC-DETR-TINYAWARE)** REFERS TO THE ENHANCED VARIANT TAILORED FOR SMALL OBJECTS. THE BEST AND SECOND-BEST RESULTS ARE HIGHLIGHTED IN **RED** AND **BLUE**, RESPECTIVELY.

Method	Publication	Input size	AP	AP ₅₀	Param	FLOPs
<i>CNN-Based</i>						
YOLOv8-L [16]	-	640×640	28.4	45.9	43.7M	165.2G
YOLOv8-X [16]	-	640×640	28.9	46.8	68.2M	257.8G
YOLOv9-M [17]	ECCV2024	640×640	25.1	41.9	20.0M	76.3G
YOLOv10-S [18]	NeurIPS2024	640×640	23.8	39.3	7.2M	21.6G
YOLOv10-L [18]	NeurIPS2024	640×640	27.6	44.6	24.4M	120.3G
YOLOv10-X [18]	NeurIPS2024	640×640	28.7	46.1	29.5M	160.4G
YOLOv11-M [19]	-	640×640	25.0	42.0	20.1M	68.0G
YOLOv11-L [19]	-	640×640	25.5	42.2	25.3M	86.9G
YOLOv11-X [19]	-	640×640	26.6	43.8	56.9M	194.9G
YOLOv12-M [20]	arXiv2025	640×640	24.4	40.9	20.2M	67.5G
YOLOv12-L [20]	arXiv2025	640×640	25.1	42.0	26.4M	88.9G
YOLOv13-L [21]	arXiv2025	640×640	24.2	40.5	27.6M	88.4G
FBRT-YOLO-M [7]	AAAI2025	640×640	28.4	45.9	7.2M	58.7G
FBRT-YOLO-L [7]	AAAI2025	640×640	29.7	47.7	14.6M	119.2G
FBRT-YOLO-X [7]	AAAI2025	640×640	30.1	48.4	22.8M	185.8G
DTSSNet [6]	TGRS2024	640×640	24.2	39.9	10.1M	49.6G
<i>Transformer-Based</i>						
Deformable DETR [23]	ICLR2020	1300×800	27.1	42.2	40.0M	173.0G
Sparse DETR [38]	ICLR2022	1300×800	27.3	42.5	40.9M	121.0G
RT-DETR-R18 [24]	CVPR2024	640×640	26.7	44.6	20.0M	60.0G
RT-DETR-R50 [24]	CVPR2024	640×640	28.4	47.0	42.0M	136.0G
Mamba-YOLO-T [39]	AAAI2025	640×640	21.0	36.8	6.0M	13.6G
Mamba-YOLO-B [39]	AAAI2025	640×640	23.9	40.8	21.8M	49.6G
DEIM-D-FINE-N [26]	CVPR2025	640×640	17.8	31.5	3.7M	7.1G
DEIM-D-FINE-S [26]	CVPR2025	640×640	24.3	40.6	10.1M	24.9G
FMC-DETR-B (Ours)	-	640×640	29.4	48.2	16.1M	56.2G
FMC-DETR-T (Ours)	-	640×640	33.2	52.8	12.6M	121.7G

TABLE II
COMPARISON OF THE PERFORMANCE OF DIFFERENT SOTA DETECTORS ON THE HAZYDET DATASET. **BOLD** INDICATES THE HIGHEST PERFORMANCE.

Model	AP	AP _{car}	AP _{truck}	AP _{bus}	Param
IAYOLO	38.3	44.1	22.2	48.6	61.8M
MS-DAYOLO	48.3	59.4	28.5	57.0	40.0M
TOOD	51.4	58.4	33.6	62.2	32.0M
Cascade RCNN	51.6	59.0	34.2	61.7	69.1M
Defrom DETR	51.5	58.4	33.9	62.3	40.0M
DeCoDet	52.0	60.5	34.0	61.9	34.6M
YOLOv12-L	52.6	57.5	37.4	62.6	26.4M
YOLOv13-L	52.7	57.5	37.6	63.1	27.6M
FMC-DETR-B	54.3	63.0	36.9	62.9	16.1M

TABLE III
COMPARISON OF THE PERFORMANCE OF DIFFERENT SOTA DETECTORS ON THE SIMD DATASET. **BOLD** INDICATES THE HIGHEST PERFORMANCE.

Model	AP	AP ₅₀	Param	FLOPs
RT-DETR-R18	63.7	78.6	19.8M	57.0G
YOLOv8-L	63.1	78.1	43.7M	165.2G
YOLOv9-M	62.2	76.6	20.0M	76.3G
Deform DETR	59.7	75.6	40.0M	196.0G
EMSD-DETR	64.3	79.4	18.4M	68.3G
HPS-DETR	63.5	79.8	15.5M	68.3G
FMC-DETR-B	65.8	80.9	16.1M	56.2G

1) *Effect of WeKat*: Introducing WeKat alone improves AP from 26.7% to 27.8%, with consistent gains in AP₅₀ (from 44.6% to 46.1%) and AP_S (from 18.5% to 19.5%). Moreover, WeKat achieves this improvement with reduced complexity,

TABLE IV
ABLATION STUDY OF OUR PROPOSED METHOD ON THE VISDRONE DATASET.

WeKat	CPF	MDFC	AP	AP ₅₀	AP _S	Param	FLOPs
✗	✗	✗	26.7	44.6	18.5	20.0M	60.0G
✓	✗	✗	27.8	46.1	19.5	16.3M	54.7G
✗	✓	✗	27.4	45.3	19.2	19.5M	55.7G
✗	✗	✓	28.2	46.6	19.7	20.4M	62.2G
✓	✓	✗	28.3	46.8	20.3	15.8M	52.0G
✓	✓	✓	29.4	48.2	21.2	16.1M	56.2G

lowering parameters from 20.0M to 16.3M and FLOPs from 60.0G to 54.7G. This demonstrates that the proposed backbone not only enhances representation learning but also offers a more efficient architecture design.

2) *Effect of CPF*: Adding CPF individually increases AP to 27.4% and AP_S to 19.2%, confirming that the cross-scale feature propagation effectively strengthens contextual interactions. While its complexity is slightly reduced compared to the baseline (FLOPs decrease from 60.0G to 55.7G), the performance gains highlight that CPF is beneficial for boosting small object detection in aerial scenarios.

3) *Effect of MDFC*: The MDFC module yields the most significant single-module improvement, raising AP to 28.2%, AP₅₀ to 46.6%, and AP_S to 19.7%. This indicates that multi-dimensional frequency context is particularly effective in capturing richer structural cues. Although MDFC introduces higher FLOPs (62.2G), the clear accuracy gains validate its contribution. When combined with WeKat and CPF, MDFC

TABLE V

ABLATION STUDY ON THE EFFECT OF $S5$ BACKBONE LAYER AND DETECTION HEAD DESIGN. “✓” AND “✗” INDICATE THE PRESENCE OR ABSENCE OF THE $S5$ STAGE, RESPECTIVELY.

Model	$S5$	Detect Layer	AP	AP_{50}	AP_{75}	AP_S	Param	FLOPs
Baseline	✓	$[D3, D4, D5]$	26.7	44.6	26.9	18.5	20.0	60.0
WeKat	✓	$[D3, D4, D5]$	27.8	46.1	28.2	19.5	16.3	54.7
WeKat	✗	$[D2, D3, D4]$	30.9	50.2	31.8	23.5	12.9	120.1
WeKat	✗	$[D3, D4]$	30.8	50.2	31.5	23.3	12.8	103.0
WeKat	✗	$[D2, D4]$	31.6	50.9	32.9	23.9	12.8	115.8
FMC-DETR-T	✗	$[D2, D3, D4]$	32.7	52.3	34.1	24.9	12.7	126.0
FMC-DETR-T	✗	$[D3, D4]$	32.1	52.0	32.9	24.0	12.6	109.0
FMC-DETR-T	✗	$[D2, D4]$	33.2	52.8	34.8	25.3	12.6	121.7

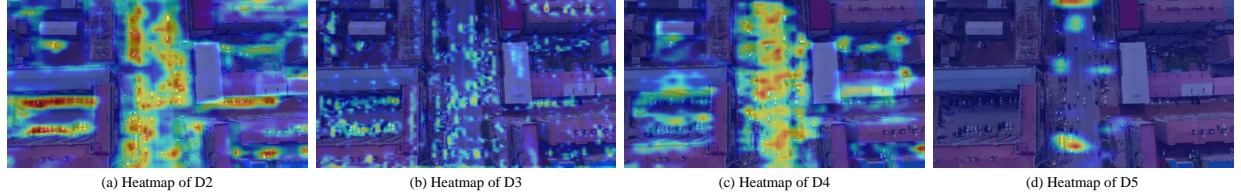


Fig. 4. Visualization of feature activations across detection layers for small objects. Here, $[D2 - D5]$ denote detection layers at different feature scales, where the spatial resolution decreases progressively by a factor of 2 at each stage.

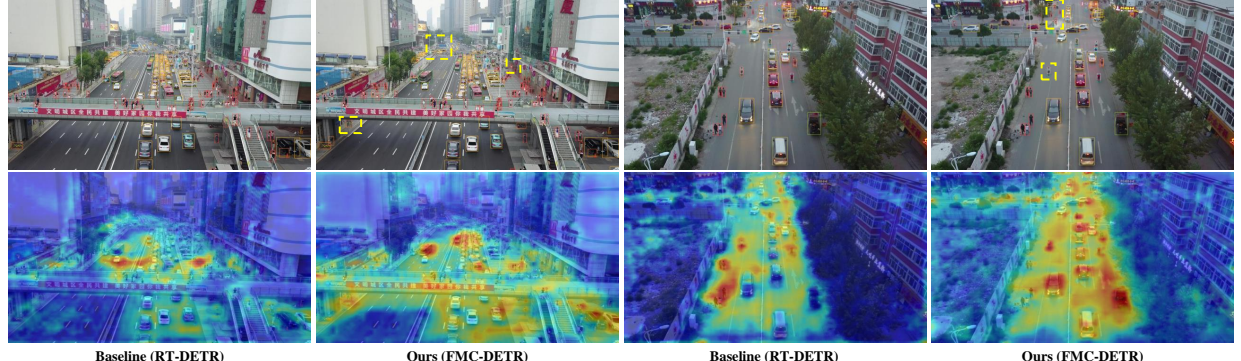


Fig. 5. Visualization of heatmaps and detection results for RT-DETR and FMC-DETR. Brighter areas in the heatmaps indicate stronger model attention.

further boosts performance to the best results of 29.4% AP, 48.2% AP_{50} , and 21.2% AP_S , demonstrating strong complementarity among all three components.

4) *Effect of Detection Layer*: In the backbone design, we investigate the necessity of the $S5$ feature layer for object detection. As the number of down-sampling operations increases, the high-frequency details of small objects are irreversibly lost, making the low-resolution $S5$ feature largely redundant for precise localization. As shown in the heatmap visualizations of different detection layers in Fig. 4, the high-resolution $D2$ layer contributes significantly more to small object detection compared to deeper layers. Motivated by this observation, we reduce one down-sampling stage in the WeKat backbone (equivalent to removing the $S5$ feature layer) and adjust the detection layers to $[D2, D3, D4]$. This modification improves the overall AP from 27.8% to 30.9%, with AP_S increasing by 4.0%, thereby validating the effectiveness of high-resolution features for small object detection. Furthermore, from the perspective of feature redundancy, different detection layers contribute unevenly to objects of varying scales. By combining this analysis with the heatmap results in Fig. 4, we find that the

$D2$ and $D4$ layers provide more sufficient and concentrated responses for small objects. Based on this insight, FMC-DETR-T ultimately adopts $[D2, D4]$ as its detection layers, achieving the best performance with 53.8% AP_{50} and 25.3% AP_S .

E. Visualization Analysis

As shown in Fig 5, we present heatmaps and detection results in the VisDrone dataset. Compare to the baseline model RT-DETR, FMC-DETR demonstrates a notably improved ability to localize small objects. Additionally, it can be observed that FMC-DETR pays more attention to the surrounding information of small objects, which demonstrates the model’s ability to better utilize contextual information during detection. To further highlight the advantages of FMC-DETR in aerial-view scenarios, we visualize both feature maps and detection outputs on the HazyDet dataset in Fig 8. The enhanced contextual understanding and clearer global structures facilitate more accurate object localization. From the visual comparisons, it is evident that our method captures both the overall object shapes and fine-grained boundaries more effectively, contributing to

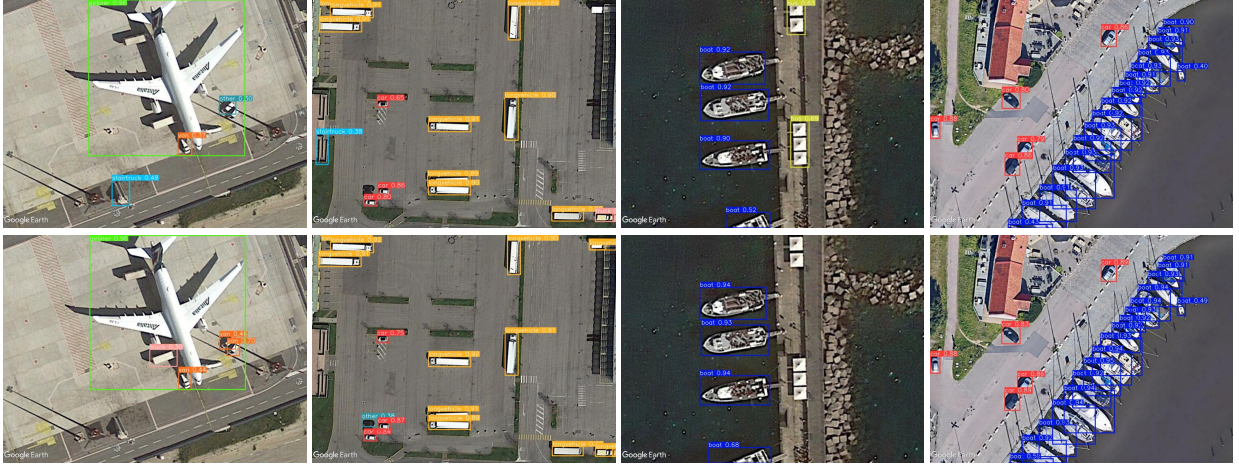


Fig. 6. Qualitative comparison of detection results on the SIMD dataset. The first row shows the predictions of the baseline model RT-DETR, while the second row presents results from the proposed FMC-DETR.

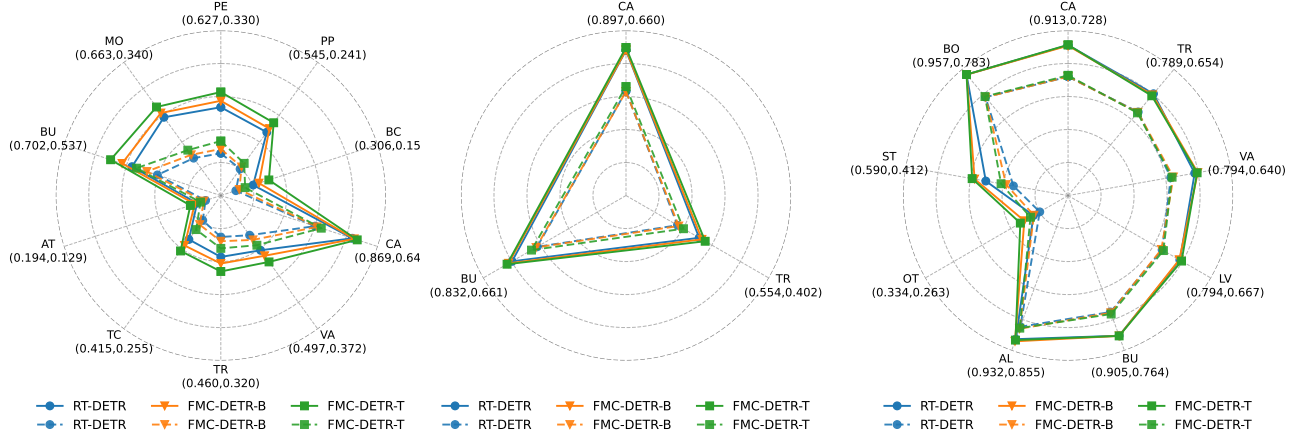


Fig. 7. Radar chart visualization of AP₅₀ and AP across categories on three datasets. From left to right are the VisDrone, HazyDet, and SIMD datasets. For the SIMD dataset, to provide a clearer illustration, we selected 9 representative categories from the original 15 by excluding rare classes with very few instances.

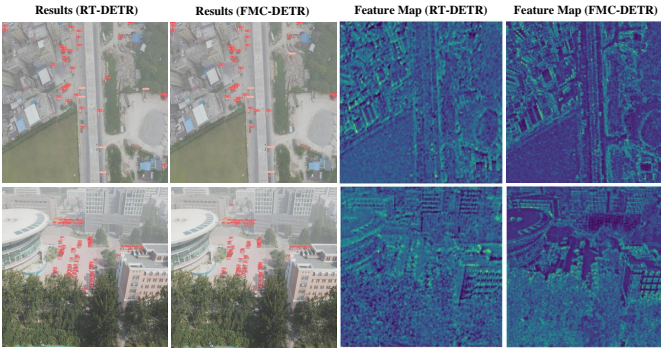


Fig. 8. Visualizations of the detection results of baseline and our proposed method on HazyDet.

its superior detection performance. In addition, we further evaluate the detection performance of FMC-DETR on the SIMD dataset. As shown in Fig 6, the qualitative results show that our method is capable of detecting more objects of interest and classifying them more accurately. These results validate the effectiveness of FMC-DETR in improving multi-object

detection accuracy, particularly in complex aerial scenes. To provide a more fine-grained comparison, we visualize per-category AP and AP₅₀ scores using radar charts across the VisDrone, HazyDet, and SIMD datasets (Fig. 7). The proposed FMC-DETR consistently shows larger and more balanced radar coverage, highlighting its superiority in handling diverse categories.

V. CONCLUSION

In this paper, we propose FMC-DETR, a detector designed for aerial-view small object detection, based on frequency decoupling and multi-domain coordination. We introduce the WeKat backbone, which enhances global low-frequency representations in the shallow layers and performs deep nonlinear modeling between deep features. We then present the CPF module, which reduces channel redundancy to improve the efficiency of multi-scale feature fusion. Finally, the MDFC module is introduced to refine feature correlations between the spatial and frequency domains, enabling the extraction of more discriminative complementary information. Extensive qualitative and quantitative experiments validate the effectiveness

of FMC-DETR, demonstrating that it achieves competitive performance with reduced parameter count and computational cost, without relying on any pretrained weights or additional training strategies.

ACKNOWLEDGMENTS

This work was supported by the National Natural Science Foundation of China under Grant 62301253, 62427818.

REFERENCES

- [1] Z. Lin, Z. Liu, Z. Xia, X. Wang, Y. Wang, S. Qi, Y. Dong, N. Dong, L. Zhang, and C. Zhu, “Rcbevdet: Radar-camera fusion in bird’s eye view for 3d object detection,” in *Proceedings of the IEEE/CVF Conference on Computer Vision and Pattern Recognition*, pp. 14928–14937, 2024.
- [2] G. Zhang, X. Ji, B. Qiu, Y. Cai, Y. Liu, X. Sui, and Q. Chen, “Sfnet: A dual-enhanced rgbt tracker via global-local modality refinement and frequency-spatial cross-modal fusion,” *Optics and Lasers in Engineering*, vol. 194, p. 109201, 2025.
- [3] J. Dong, J. Feng, and X. Tang, “Optisar-net: A cross-domain ship detection method for multi-source remote sensing data,” *IEEE Transactions on Geoscience and Remote Sensing*, 2024.
- [4] H. Wei, N. Wang, Y. Liu, P. Ma, D. Pang, X. Sui, and Q. Chen, “Spatio-temporal feature fusion and guide aggregation network for remote sensing change detection,” *IEEE Transactions on Geoscience and Remote Sensing*, 2024.
- [5] B. Du, Y. Huang, J. Chen, and D. Huang, “Adaptive sparse convolutional networks with global context enhancement for faster object detection on drone images,” in *Proceedings of the IEEE/CVF conference on computer vision and pattern recognition*, pp. 13435–13444, 2023.
- [6] L. Chen, C. Liu, W. Li, Q. Xu, and H. Deng, “Dttsnet: Dynamic training sample selection network for uav object detection,” *IEEE transactions on geoscience and remote sensing*, vol. 62, pp. 1–16, 2024.
- [7] Y. Xiao, T. Xu, Y. Xin, and J. Li, “Fbrt-yolo: Faster and better for real-time aerial image detection,” in *Proceedings of the AAAI Conference on Artificial Intelligence*, vol. 39, pp. 8673–8681, 2025.
- [8] S. Deng, S. Li, K. Xie, W. Song, X. Liao, A. Hao, and H. Qin, “A global-local self-adaptive network for drone-view object detection,” *IEEE Transactions on Image Processing*, vol. 30, pp. 1556–1569, 2020.
- [9] L. Min, Z. Fan, Q. Lv, M. Reda, L. Shen, and B. Wang, “Yolo-dcti: small object detection in remote sensing base on contextual transformer enhancement,” *Remote Sensing*, vol. 15, no. 16, p. 3970, 2023.
- [10] A. Vaswani, N. Shazeer, N. Parmar, J. Uszkoreit, L. Jones, A. N. Gomez, Ł. Kaiser, and I. Polosukhin, “Attention is all you need,” *Advances in neural information processing systems*, vol. 30, 2017.
- [11] A. Dosovitskiy, L. Beyer, A. Kolesnikov, D. Weissenborn, X. Zhai, T. Unterthiner, M. Dehghani, M. Minderer, G. Heigold, S. Gelly, et al., “An image is worth 16x16 words: Transformers for image recognition at scale,” *arXiv preprint arXiv:2010.11929*, 2020.
- [12] Z. Liu, Y. Lin, Y. Cao, H. Hu, Y. Wei, Z. Zhang, S. Lin, and B. Guo, “Swin transformer: Hierarchical vision transformer using shifted windows,” in *Proceedings of the IEEE/CVF international conference on computer vision*, pp. 10012–10022, 2021.
- [13] Y. Cao, Z. He, L. Wang, W. Wang, Y. Yuan, D. Zhang, J. Zhang, P. Zhu, L. Van Gool, J. Han, et al., “Visdrone-det2021: The vision meets drone object detection challenge results,” in *Proceedings of the IEEE/CVF International conference on computer vision*, pp. 2847–2854, 2021.
- [14] C. Feng, Z. Chen, X. Li, C. Wang, J. Yang, M.-M. Cheng, Y. Dai, and Q. Fu, “Hazydet: Open-source benchmark for drone-view object detection with depth-cues in hazy scenes,” *arXiv preprint arXiv:2409.19833*, 2024.
- [15] M. Haroon, M. Shahzad, and M. M. Fraz, “Multisized object detection using spaceborne optical imagery,” *IEEE Journal of Selected Topics in Applied Earth Observations and Remote Sensing*, vol. 13, pp. 3032–3046, 2020.
- [16] G. Jocher, A. Chaurasia, and J. Qiu, “Ultralytics yolov8,” 2023.
- [17] C.-Y. Wang, I.-H. Yeh, and H.-Y. Mark Liao, “Yolov9: Learning what you want to learn using programmable gradient information,” in *European conference on computer vision*, pp. 1–21, Springer, 2024.
- [18] A. Wang, H. Chen, L. Liu, K. Chen, Z. Lin, J. Han, et al., “Yolov10: Real-time end-to-end object detection,” *Advances in Neural Information Processing Systems*, vol. 37, pp. 107984–108011, 2024.
- [19] G. Jocher and J. Qiu, “Ultralytics yolo11,” 2024.
- [20] Y. Tian, Q. Ye, and D. Doermann, “Yolov12: Attention-centric real-time object detectors,” *arXiv preprint arXiv:2502.12524*, 2025.
- [21] M. Lei, S. Li, Y. Wu, H. Hu, Y. Zhou, X. Zheng, G. Ding, S. Du, Z. Wu, and Y. Gao, “Yolov13: Real-time object detection with hypergraph-enhanced adaptive visual perception,” *arXiv preprint arXiv:2506.17733*, 2025.
- [22] N. Carion, F. Massa, G. Synnaeve, N. Usunier, A. Kirillov, and S. Zagoruyko, “End-to-end object detection with transformers,” in *European conference on computer vision*, pp. 213–229, Springer, 2020.
- [23] X. Zhu, W. Su, L. Lu, B. Li, X. Wang, and J. Dai, “Deformable detr: Deformable transformers for end-to-end object detection,” *arXiv preprint arXiv:2010.04159*, 2020.
- [24] Y. Zhao, W. Lv, S. Xu, J. Wei, G. Wang, Q. Dang, Y. Liu, and J. Chen, “Dets beat yolos on real-time object detection,” in *Proceedings of the IEEE/CVF conference on computer vision and pattern recognition*, pp. 16965–16974, 2024.
- [25] Y. Peng, H. Li, P. Wu, Y. Zhang, X. Sun, and F. Wu, “D-fine: Redefine regression task in dets as fine-grained distribution refinement,” *arXiv preprint arXiv:2410.13842*, 2024.
- [26] S. Huang, Z. Lu, X. Cun, Y. Yu, X. Zhou, and X. Shen, “Deim: Detr with improved matching for fast convergence,” in *Proceedings of the Computer Vision and Pattern Recognition Conference*, pp. 15162–15171, 2025.
- [27] Z. He, W. Ran, S. Liu, K. Li, J. Lu, C. Xie, Y. Liu, and H. Lu, “Low-light image enhancement with multi-scale attention and frequency-domain optimization,” *IEEE Transactions on Circuits and Systems for Video Technology*, vol. 34, no. 4, pp. 2861–2875, 2023.
- [28] Z. Wang, Y. Zhang, Y. Liu, D. Zhu, S. A. Coleman, and D. Kerr, “Elwnet: An extremely lightweight approach for real-time salient object detection,” *IEEE Transactions on Circuits and Systems for Video Technology*, vol. 33, no. 11, pp. 6404–6417, 2023.
- [29] K. Li, D. Wang, Z. Hu, W. Zhu, S. Li, and Q. Wang, “Unleashing channel potential: Space-frequency selection convolution for sar object detection,” in *Proceedings of the IEEE/CVF Conference on Computer Vision and Pattern Recognition*, pp. 17323–17332, 2024.
- [30] X. Ding, X. Zhang, J. Han, and G. Ding, “Scaling up your kernels to 31x31: Revisiting large kernel design in cnns,” in *Proceedings of the IEEE/CVF conference on computer vision and pattern recognition*, pp. 11963–11975, 2022.
- [31] Z. Liu, Y. Wang, S. Vaidya, F. Ruehle, J. Halverson, M. Soljačić, T. Y. Hou, and M. Tegmark, “Kan: Kolmogorov-arnold networks,” *arXiv preprint arXiv:2404.19756*, 2024.
- [32] X. Yang and X. Wang, “Kolmogorov-arnold transformer,” *arXiv preprint arXiv:2409.10594*, 2024.
- [33] Y. Ioannou, D. Robertson, R. Cipolla, and A. Criminisi, “Deep roots: Improving cnn efficiency with hierarchical filter groups,” in *Proceedings of the IEEE conference on computer vision and pattern recognition*, pp. 1231–1240, 2017.
- [34] A. G. Howard, M. Zhu, B. Chen, D. Kalenichenko, W. Wang, T. Weyand, M. Andreetto, and H. Adam, “Mobilennets: Efficient convolutional neural networks for mobile vision applications,” *arXiv preprint arXiv:1704.04861*, 2017.
- [35] J. Chen, S.-h. Kao, H. He, W. Zhuo, S. Wen, C.-H. Lee, and S.-H. G. Chan, “Run, don’t walk: chasing higher flops for faster neural networks,” in *Proceedings of the IEEE/CVF conference on computer vision and pattern recognition*, pp. 12021–12031, 2023.
- [36] Q. Zhang, Z. Jiang, Q. Lu, J. Han, Z. Zeng, S.-H. Gao, and A. Men, “Split to be slim: An overlooked redundancy in vanilla convolution,” *arXiv preprint arXiv:2006.12085*, 2020.
- [37] K. Han, Y. Wang, Q. Tian, J. Guo, C. Xu, and C. Xu, “Ghostnet: More features from cheap operations,” in *Proceedings of the IEEE/CVF conference on computer vision and pattern recognition*, pp. 1580–1589, 2020.
- [38] B. Roh, J. Shin, W. Shin, and S. Kim, “Sparse detr: Efficient end-to-end object detection with learnable sparsity,” *arXiv preprint arXiv:2111.14330*, 2021.
- [39] Z. Wang, C. Li, H. Xu, X. Zhu, and H. Li, “Mamba yolo: A simple baseline for object detection with state space model,” in *Proceedings of the AAAI Conference on Artificial Intelligence*, vol. 39, pp. 8205–8213, 2025.
- [40] C. Zhang and J. Yang, “Emsd-detr: efficient small object detection for uav aerial images based on enhanced rt-detr model,” *The Journal of Supercomputing*, vol. 81, no. 9, pp. 1–33, 2025.
- [41] X. Wang and H. Chen, “Hps-detr: Enhancing small object detection with lightweight feature extraction and transformer integration,” *Authorea Preprints*, 2025.